Published in final edited form as:
J Proteome Res. 2011 September 2; 10(9): 4134–4149. doi:10.1021/pr200313x.

The Fasted/Fed Mouse Metabolic Acetylome: N6-Acetylation Differences Suggest Acetylation Coordinates Organ-Specific Fuel Switching

Li Yang[1,§], **Bhavapriya Vaitheesvaran**[2,§], **Kirsten Hartil**[2], **Alan J. Robinson**[3], **Michael R. Hoopmann**[4], **Jimmy K. Eng**[5], **Irwin J. Kurland**[2], and **James E. Bruce**[4]

[1]Department of Chemistry, Washington State University, Pullman, Washington, 99164

[2]Department of Medicine, Stable Isotope and Metabolomics Core Facility, Albert Einstein College of Medicine Diabetes Center, Bronx, New York, 10461

[3]Medical Research Council Mitochondrial Biology Unit, Cambridge, CB2 0XY, United Kingdom

[4]Department of Genome Sciences, University of Washington, Seattle, Washington, 98109

[5]University of Washington Proteomics Resource, Seattle, Washington, 98109

Abstract

The elucidation of extra-nuclear lysine acetylation has been of growing interest, as the co-substrate for acetylation, acetyl CoA, is at a key metabolic intersection. Our hypothesis was that mitochondrial and cytoplasmic protein acetylation may be part of a fasted/re-fed feedback control system for the regulation of the metabolic network in fuel switching, where acetyl CoA would be provided by fatty acid oxidation, or glycolysis, respectively. To test this we characterized the mitochondrial and cytoplasmic acetylome in various organs that have a high metabolic rate relative to their mass, and/or switch fuels, under fasted and re-fed conditions (brain, kidney, liver, skeletal muscle, heart muscle, white and brown adipose tissues). Using immunoprecipitation, coupled with LC-MSMS label free quantification, we show there is a dramatic variation in global quantitative profiles of acetylated proteins from different organs. In total, 733 acetylated peptides from 337 proteins were identified and quantified, out of which 31 acetylated peptides from the metabolic proteins that may play organ-specific roles were analyzed in detail. Results suggest that fasted/re-fed acetylation changes coordinated by organ-specific (de-)acetylases in insulin-sensitive versus insensitive organs may underlie fuel use and switching. Characterization of the tissue-specific acetylome should increase understanding of metabolic conditions wherein normal fuel switching is disrupted, such as in Type II diabetes.

Introduction

The function and physical properties of proteins can be regulated by protein post-translational modifications (PTMs). Lysine acetylation is a reversible PTM that affects a variety of biological processes, such as protein-DNA interactions, enzyme activation/inactivation, subcellular localization and protein stability, *etc* [1, 2]. In the past four decades, histones have been the primary focus of acetylation studies because of their high abundance

Corresponding authors: Irwin J. Kurland and James E. Bruce, Current address: Department of Medicine, Stable Isotope and Metabolomics Core Facility, Albert Einstein College of Medicine Diabetes Center, Bronx, New York, 10461 and Department of Genome Sciences, University of Washington, Seattle, Washington, 98109., jimbruce@u.washington.edu, Phone: 206-543-0220, Fax: 206-616-0008, Irwin.kurland@einstein.yu.edu, Phone 718-678-1180, Fax: 718-678-1020.
§These authors contributed equally to the paper

and high frequency of lysine acetylation. Only studies of specific acetylation in individual proteins were possible in the past due to the lack of robust detection technologies[3–5]. Improvements of modern mass spectrometers, specifically improved accurate mass detection, sensitivity and dynamic range, higher resolution, and faster scan rates, all serve to greatly facilitate global acetylation studies[6] as has been reported recently[7–9]. In 2006, Kim *et al*. published the first proteome-wide report by using immunoprecipitation enrichment of acetylated peptides with an anti-acetylated lysine antibody and HPLC-MSMS detection[8] to identify 195 acetylated proteins from mouse liver. Choudhary *et al*. and Zhao *et al*. advanced this approach and demonstrated the largest data set of acetylated peptides identified from human cells (1750 acetylated proteins) and liver tissue (1047 acetylated proteins)[7, 9]. These reports show large numbers of acetylated non-histone proteins, many of which are mitochondrial or cytoplasmic species. Thus, lysine acetylation is involved in a greater diversity of functional roles and subcellular localizations than previously recognized.

As lysine acetylation is dynamic and regulates protein function in ways not fully understood, global quantitative analyses of lysine acetylation are critical to better understand the functional impact and use of this modification in biological systems. For example, Kendrick *et al*. showed fatty liver was associated with reduced sirtuin activity and increased acetylation levels of mitochondrial proteins[10]. They isolated acetylated proteins from total liver proteome samples from mice on a high fat diet (HFD, 4 months) and control animals. Acetylated proteins were immunoprecipitated with immobilized anti-acetylated lysine antibodies, purified proteins were separated on 1-D gels, scanned, and relative quantification between HFD-fed and control animal samples was performed. Bands that exhibited significant differential staining between HFD and control samples were subjected to in-gel digestion and mass spectrometry analysis. In total, 193 proteins were differentially acetylated in HFD samples, including proteins involved in gluconeogenesis, mitochondrial protein oxidation, methionine metabolism, liver injury and endoplasmic reticulum stress response. Importantly, the work of Kendrick *et al.* shows that differences in levels of acetylated liver proteins relevant to altered feeding status in mice can be observed by proteomic methods. Previously, Choudhary *et al.* used SILAC (Stable isotope labeling with amino acids in cell culture)[7] and Zhao *et al.* used iTRAQ labeling (isobaric tag for relative and absolute quantification)[9] coupled with LC-MSMS techniques to quantify peptide-level, or site-specific acetylation in human cell lines and liver tissue respectively. Schwer and co-workers[11] reported label free quantification (LFQ) of the acetylated peptides from mouse liver tissue. LFQ technology is beneficial for studies of live animal tissues because incorporation of heavy isotopes is not required. In this way, Schwer *et al*. studied how calorie restriction (CR) can alter the mitochondrial protein acetylation levels in mouse liver. Approximately 300 proteins were quantified, and 72 were determined to have at least a 2.5 fold change in acetylation during CR. SILAM (Stable Isotope Labeling in Mammals)[12] can in principle allow isotope incorporation in these studies with live animal tissues, although the additional expense significantly limits the applicability. In this work, a further advance of these approaches includes measurement of differences of acetylation on specific peptides by quantitative LC-MSMS methods, and comparison of level changes observed among several tissues or organs.

Acetylation is dynamic and cellular acetylation status is dependent on the activities of acetylases and deacetylases. Intracellular acetyl CoA, used by acetylases, sits on the metabolic crossroads of glycolysis, fatty acid oxidation, ketogenesis, amino acid metabolism, and TCA cycle utilization for ATP synthesis, making acetyl CoA an ideal quantity for sensing (via the non-nuclear acetylome) metabolic network function. Intracellular NAD^+/NADH ratio, a central determinant of nutritional status also critically regulates the activity of NAD^+ deacetylases. Metabolic inflexibility, or the inability of an organism to adapt and modify fuel oxidation in response to changes in nutrient availability,

is characteristic of dysfunction seen in metabolic syndrome and Type II Diabetes[13–18]. The hypothesis for this study is that fasted/re-fed characterization of the organ specific mitochondrial and cytoplasmic acetylome may yield insights into both normal functional roles of tissue specific fuel switching, as well as abnormalities seen in situations, like diabetes mellitus, where metabolic inflexibility is evident. Therefore, analyzing the acetylation pattern of major mammalian tissues that greatly differ metabolically and play a diverse role in energy homeostasis under different nutritional status would be highly informative. Previous studies have reported murine fasted and re-fed hepatic acetylome only[8]. Our efforts in this study focus on the characterization of the fasted/re-fed acetylome patterns of tissues that are known to switch fuels between the fasted/fed states (liver, skeletal muscle, heart muscle, white adipose and brown adipose) or have a high metabolic rate relative to their mass (brain and kidney)[19]. No one organ is responsible for the metabolic rate, but some organs (brain, kidney, heart, and gastrointestinal tract) contribute a much larger fraction of their metabolic rate than their fractional mass or volume of the body, whereas others (bone, white adipose tissue, skin, and skeletal muscle) contribute much less[19]. Brown adipose tissue contributes to the metabolic rate in neonatal mammals, and small mammals adapted to cold environments[21]. Metabolic consequences of the presence or absence of the thermogenic capacity of brown adipose tissue in mice has been reported[21, 22], so brown adipose was also used for this study; white adipose tissue was included for comparison. The metabolic rate may fall 10% during sleep, a normal fasted condition, and may fall by 40% during long-term starvation in humans[20], supporting the relevance of acetylome changes on energy metabolism found for metabolic network enzymes during dietary shifts.

In this study, the acetylation levels of peptides from mitochondrial proteins in each tissue under differential feeding status were of primary interest. In total, 733 acetylated peptides from 337 proteins were identified, out of which the levels of 58 acetylated peptides changed 3-fold or greater under fasted/re-fed conditions. These peptides constitute the top 5% largest changes in acetylation levels among the 733 acetylated peptides, based on two standard deviations from the center of the observed $\log_{10}$ (re-fed/fasted) distribution as a cut off. Thirty-one acetylated peptides of these 58 are from metabolic proteins or chaperones. Many of these protein acetylation events may be relevant metabolic changes that accompany fuel switching and will serve as targets for future investigation. Our results show that acetylation levels in ATP-generating or utilizing metabolic processes such as glycolysis, Krebs cycle, gluconeogenesis, lipid synthesis and oxidation likely serve as control points or play a role in modulation of these pathways. In fact, acetylation is a classic candidate for such critical regulation, owing to its requirement of acetyl CoA, an important intermediate molecule linking such major pathways, as its acetyl group donor. The results presented here are first to demonstrate that there variation exists in the global quantitative profiles of acetylated metabolic proteins in all these organs, that are dramatically affected by comparison of the fasted to re-fed state.

Materials and Methods

1. Materials

Deacetylase inhibitors (TSA, Nicotinamide, Butyric acid), 2,2,2-Trifluoroethanol (TFE), Ammonium bicarbonate (ABC), Iodoacetamide (IAA) and Tergitol solution (70% NP40 in water) were purchased from Sigma-Aldrich (St. Louis, MO) and used without purification.

Affinity-purified anti-acetyl lysine antibody immobilized onto protein A-conjugated agarose beads was purchased from ImmunoChem Pharmaceuticals Inc. (Burnaby, British Columbia, Canada). TCEP, BupH™ Tris Buffered Saline Pack (IP buffer), BCA Protein Assay Kit and mass spectrometry-grade Trypsin endoproteinase were purchased from Pierce (Rockford, IL,

USA). Protease inhibitor cocktail tablets were purchased from Roche Diagnostics (Indianapolis, IN, USA).

2. Animals

Four to five months old male FVB/N background mice studied were housed in a full-barrier facility with a 12-hour light/dark cycle (7:00 am/7:00 pm) throughout the study. Animals had full access to food (standard chow from Harlan Teklad 4% Mouse/Rat Diet cat # 7001) and water unless otherwise stated. All animal experiments were performed in accordance with National Institutes of Health guidelines and with the approval of the Animal Care and Use Committee of Albert Einstein College of Medicine. For the fasting/re-feeding studies, mice were allowed to eat for an hour and half after the beginning of the dark cycle (7:00 pm) and fasting was initiated by removing the food at 8:30 pm. Animals (n=5) were sacrificed the next day at the end of: a) 18 hours fast (2:30 pm) for fasting studies, b) 13 hours fast (9:30 am) followed by 5 hours re-feeding (2:30 pm) for re-feeding studies. Harvested tissues (liver, brown adipose, white adipose, heart muscle, skeletal muscle, kidney and brain) were snap-frozen in liquid N_2 and stored at −80° C until further analysis.

3. Sample preparation

Matching tissues or organs from five mice were pooled together. Pooling the samples from different biological sources has been shown to reduce the biological variation, as one might anticipate, and in many cases, increases the ability to study the differences caused by treatment as described in several references [46–48]. Because of limited sample sizes available in a single animal, pooled samples were required to study all seven tissues presented here. Sample preparation was divided into: 1) Tissue protein extraction, 2) normalization and tryptic digestion and 3) the enrichment of the acetylated peptides. A general experimental scheme is shown in Figure 1. Tissues were homogenized in the lysis buffer, which contains 50% TFE, 0.1M ABC, 5mM TCEP, 10μM TSA, 10 mM nicotinamide, 50mM butyric acid and protease inhibitor cocktail. The pH of the lysis buffer was adjusted to 7.4. Minimal volume of the lysis buffer was used in the homogenizing step to get highly concentrated protein solutions. The samples were sonicated to reduce the viscosity and heated at 99 °C for 5 min. The protein solutions were centrifuged at 16,000 × G for 20 min to separate solids. Protein concentration in the supernatant portions was measured with a BCA protein quantification kit. All samples were normalized by using an aliquot containing the same amount of total protein. Thirty milligrams of protein from each sample were reduced and alkylated with a final concentration of 50mM TCEP and IAA, respectively. The volume of each sample was diluted 5 times with 100 mM ABC buffer; and the pH was adjusted to 8–8.2. The samples were then subjected to digestion with trypsin with a 500:1 protein-to-enzyme ratio and were incubated overnight at 37 °C. Then the mixtures were heated at 99 °C for 5 min to denature trypsin and reduce activity. The mixtures were centrifuged at 16,000 × G for 2 min; and the supernatants were separated from the insoluble fractions. TFE was evaporated from the supernatants which were placed under vacuum (Thermo Speed Vacuum SPD131DDA). We previously found 0.1% concentration of the non-ionic detergent NP40 to be optimal for immunoprecipitation[23] so this was the final concentration of NP40 used here, and the pH was adjusted to 7.4. For each 30 mg of digested protein sample, a 200 μL slurry aliquot of the anti-acetylated lysine antibody beads was used for immunoprecipitation. The aliquots of the antibody slurry were washed with phosphate buffered saline (PBS) 3 times, and then added into the peptide solutions. The mixtures were then incubated 3 hours at 4 °C, centrifuged and the antibody beads were separated from the supernatants. The beads were washed 4 times with IP buffer and eluted with a 100 μL of the elution buffer 3 times (0.1% formic acid and 50% acetonitrile in DI water). Then the eluents were dried under vacuum and re-dissolved in a 20 μL buffer of 0.1% formic acid in DI water.

4. Mass spectrometric analyses

The enriched acetylation products were fractionated with UPLC (nanoAcquity Waters, Milford, MA) and analyzed with a built-in-house Velos-FT mass spectrometer[24] (Submitted to Analytical Chemistry). The FT analyzer enables high resolution and accurate mass detection and the Velos mass spectrometer allows fast scan speed and better sensitivity, which is important for the identification of the low abundance acetylated peptides. A 35 cm long C18 column was made in house by packing fused silica capillary (360 μm × 75 μm) with MAGIC C18AQ 100A 5U beads (Michrom Bioresources, Inc., Auburn, CA). The electrospray ionization (ESI) tip was made by pulling the end of the column with a laser puller (Model P-2000, Sutter Instrument Co.). A 2 cm long trap column was prepared similarly by packing a frit fused silica capillary (360 μm × 100 μm) with MAGIC C18AQ 200A 5U beads. The following LC gradient was used: 0–60 min 5%–35% buffer B, 60–75 min flushing with 80% buffer B and 75–100 min equilibrating with 5% buffer B. Buffer A and buffer B consisted of 0.1% formic acid, 0.1% formic acid and 95% acetonitrile in DI water, respectively. One MS measurement in the FT analyzer with 25K resolving power was followed by 10 MSMS measurements in DDA mode in the Velos instrument. The dynamic exclusion repeat and the exclusion duration were 15 sec. Each sample was analyzed in triplicate and in each analysis 5 μL of sample solution was loaded onto the column. Two LC-MSMS measurements of a mixture of 0.5 pmol angiotension I and neurotensin were run after the triplicate analyses of each sample. The first run was used to clean the column, and the second run was used to verify the column performance. A total of 42 LC-MSMS experiments with mouse tissue and organ samples were acquired, and used to quantify acetylated peptides.

5. Data analyses

Peptide identification—The obtained LC-MSMS data were searched against the mouse database (IPI_mouse_3.26) with Mascot (version: 2.3.01). The parameters in database search were: missed cleavage = 3, precursor error tolerance = 15 ppm, fragmentation error tolerance = 0.6 Da, fixed modification of carbamidomethyl on cysteine, variable modifications of acetylation on lysine and oxidation on methionine. The false discovery rate (FDR) was determined in Mascot by enabling decoy database search [44, 45]. The acetylated sites are assigned both by Mascot search and manual verification. In most cases, only a single possible modification site (internal lysine residue) exists in the peptide sequence, yielding unambiguous acetylation site assignment. In cases where multiple possible acetylation sites were assigned by Mascot, manual verification of the MS/MS fragmentation patterns was used to determine acetylation sites. The mass error distribution between the observed and the theoretical masses of all identified peptides from the fasted and re-fed samples are plotted in Supplementary Figure 1. The center and standard deviation of the acetylated peptide mass error distribution is at 3.5 ppm and 5 ppm, respectively. Many non-specific binding peptides were identified even after immunoprecipitation, which indicates mass spectrometric fragmentation and database search identification of the peptides are necessary to distinguish the acetylated and non-acetylated peptides. Importantly, protease digestion of total cellular extracts prior to IP, and LC-MSMS analysis of acetylated peptides, presents an additional level of specificity in the analysis of global acetylation as compared to the IP of acetylated proteins, since non-specific binders are readily distinguished during the database search (reviewed in Guan and Xiong[32]). For example, the use of variable acetyl modification on lysine side chains during database search allows differentiation of nonspecific binding peptides and *bona fide* acetylated lysine-containing peptides. On the other hand, in the analysis of immunoprecipitated acetylated proteins, non-acetylated peptides could originate from either specific or non-specific binders which can complicate the analysis. Non-specific binding proteins could show different abundances after immunoprecipitation and mistakenly be considered as differentially acetylated proteins

without mass spectrometry identification of the actual acetylated peptides. In addition, protease digestion of total cellular extracts prior to IP exposes a greater amount of acetylated lysine residues and significantly helps to enrich the acetylated peptides. This was seen by our increased identification of organ specific acetylated proteins in comparison to studies where spots identified as having increased acetylation are cut out of 1-D or 2-D gels, and trypsin cleavage is done in gel, followed by extraction of the digested tryptic peptides[10, 25].

Label free quantification of the acetylated peptides—Custom software written in-house called Phosphoman was used for quantification of the acetylated peptides from multiple samples. Phosphoman was written to enable quantification of peptide results with Mascot, the existing database search algorithm used in our lab. The data analysis workflow consists of three major functions including: 1) chromatographic alignment of multiple sample injections, 2) assignment of peptide sequence identifications to their respective precursor ion signals, and 3) quantitative analysis of the peptide signals across all data sets. Each of these functions is described in detail below.

Chromatographic alignment of multiple sample injections: Peptide isotope distributions from the primary spectra of each run were identified using the feature detection software, Hardklör[26], with a correlation cutoff of 0.9. Persistent peptide isotope distributions (PPIDs) were acquired for each run by tracing the peptide signals identified with Hardklör that persisted over at least three consecutive spectra (allowing for a single gap) with a 10 ppm monoisotopic mass tolerance. For each scan event in which a persistent signal was observed, the retention time and signal intensity were recorded to create a chromatographic profile for that PPID. The list of PPIDs for each run could then be aligned with each other by matching mass within 10 ppm and retention time overlap with a 3 minute tolerance.

Assignment of peptide sequence identifications: Because the mass spectra were acquired using shotgun methods, a single peptide sequence database was assembled from the pooled database searching results for all the samples being compared. For a peptide sequence to be accepted into the database, it must be observed in at least one run with a consistent chromatographic elution profile. PPIDs were assigned a peptide sequence from the database if the monoisotopic masses matched within 10 ppm and were within the range of observed retention times with a 3 minutes tolerance.

Quantitative analysis of the peptide signals: Differences in peptide signal abundance levels were compared across the different samples analyzed with Phosphoman. The peptide signal intensity at each scan event of a PPID was summed together to obtain a measurement of the extracted ion chromatographic (EIC) peak area for that PPID. All the peptides were used for alignment, however only the modified one were analyzed quantitatively. A scheme of data analysis is shown in Figure 1b.

Study of the deviation with an internal standard—The deviation caused by sample preparation and mass spectrometric analyses was carefully studied. An acetylated BSA sample was prepared as described in a previous report[27]. An equal amount (15 picomoles) of the acetylated BSA protein was spiked into each mouse liver sample before the samples were subjected to trypsin digestion. Therefore, equal amounts of the acetylated BSA peptides were used as internal standards. Supplementary Figure 2 shows the quantification results of all the identified acetylated BSA peptides, with sequences indicated. Good overall reproducibility of the experiment is observed. None of the acetylated BSA peptide $\log_{10}$ ratios fall outside $\pm 2\sigma$ of the distribution of $\log_{10}$ (re-fed/fasted) of liver samples. The averaged EIC area observed from the re-fed sample is 1.1-fold of that from the fasted sample and the averaged standard deviation in measured BSA peptide PPID areas is 18%.

Results

1. Label free quantification

Once an acetylated peptide was identified in one LC-MSMS run, a mass-and-time tag was given to the peptide to allow its identification in the other LC-MSMS measurements with the same accurate mass (≤ 10 ppm) and retention time (± 1.5 min)[28]. For LFQ analyses, EIC peak areas of each acetylated peptide were compared between different LC-MSMS experiments. Figure 2 illustrates an example of the acetylated peptide from hydroxymethylglutaryl-CoA lyase that was identified. The acetylated peptide was identified by using the LC-MSMS data from the fasted liver sample (Figure 2a). Accurate mass and retention time was used to extract the specific peptide's EICs from the other LC-MSMS runs. Figure 2b was generated with the software Xcalibur with a mass error tolerance of 0.01 Da (< 10 ppm) to illustrate how quantification with Phosphoman was achieved. Phosphoman does not yield graphical data, but reports only numerical quantification results. Between different runs, the observed retention time variance is less than 1 minute, which demonstrates good reproducibility of the LC performance. Integrated EIC peak areas are listed as "AA" values on top of each EIC peaks. Six EIC traces are from the triplicate runs of the fasted and re-fed liver tissues respectively. The average areas and standard deviations were calculated from each group of the triplicate runs. In this case, the average of the fasted liver sample area is 1.24×10^8 (in arbitrary units) and the standard deviation is 1.36×10^7; while the average of the re-fed liver sample is 1.17×10^8 and the standard deviation is 0.72×10^7. In addition, Figure 2c shows the quantification results of an acetylated peptide (FCVGLQK@IEEIFKK) that was found to be altered in abundance (3-fold or greater) with feeding status. The average peak area of the peptide under the fasting condition is 1.23×10^7 with a standard deviation of 1.91×10^6, and that under the re-feeding condition is 1.31×10^6 with a standard deviation of 4.66×10^5. In this study, 733 acetylated peptides like this example were identified and automatically quantified in the LFQ approach with the software Phosphoman. For comparison with existing methods, data obtained from fasted liver samples were also analyzed with the published software MaxQuant[29]. The relative peak areas (area of a specific peptide/the most abundant peptide's area) and the standard deviations were calculated with the two software tools respectively (Supplementary Table 1). For most peptides, good agreement in calculated peak areas and standard deviation values was observed between Phosphoman and MaxQuant results.

2. Mouse acetylome

Here, the acetylome of seven vital mouse tissues harvested under different physiological conditions (fasting and re-feeding) are reported. Unique peptides identified from protein groups were clustered together and treated as a single entry. Peptides that have the same sequence and modification but were reported by Mascot to be modified at different residues were validated by manual inspection of the specific MSMS fragments that are unique to the modification positions. Validated peptides with a common sequence but modifications at different sites are treated as different entries in the table. An index number was given to each entry. Multiple acetylated peptides from the same protein were grouped in the list, so they have neighboring index numbers. A total of 733 non-redundant acetylated peptides from 337 mouse proteins were identified with a false discovery rate (FDR) less than 1.5% (Supplementary Table 2), which constitutes the largest mouse acetylome dataset produced to date. Previously, Kim *et al.* and Schwer *et al.* reported 195 and 287 acetylated proteins from mouse liver tissues[8, 11] and our results have 31 and 86 proteins in common with these previous reports, respectively.

3. Tissue specific acetylome profiles

A goal of this study was to investigate the acetylation sites observed in multiple mouse tissues and organs and to quantify acetylation level changes upon fasting to re-fed transition. Thus, a challenge in the analysis was to visualize a large number of acetylation sites, how they changed with feeding status, and how they did so across tissue types or organs. To achieve a comparison that can be more readily visualized, a reduced number of identified acetylated peptides are displayed from 23 metabolic and chaperone proteins. Since this work involved a fasting to re-fed transition, metabolic proteins were considered most relevant for the comparison across multiple organs, and these 21 metabolic and 2 chaperone proteins were selected based on prior knowledge of function. Selection of peptides from this set of proteins resulted in 127 acetylated peptides (Table 1). Each panel in Figure 3 illustrates one organ-specific acetylome profile of the 23 selected proteins identified in these experiments, where extracted ion chromatographic peak areas from each peptide were derived through analysis with Phosphoman and were used for quantification. In each panel, all signals were normalized to the most abundant acetylated peptide from this subset observed in that tissue or organ, and standard deviations were calculated from triplicate LC-MSMS experiments. Peptides from the same protein are grouped and shaded with white or gray background. The selected 23 proteins are indicated with single letters on top of each group of peptides and the protein names are listed in Figure 3. Acetylation sites on several peptides were observed to be common across different tissues. For example, peptides 23 and 24 from ATP synthase coupling factor 6 (F_6) have high abundance in all the samples, regardless of tissue types and feeding status. However in many other cases, the same acetylated peptide shows remarkably different abundance levels in different tissues (see Discussion). For example, these include acetylated peptides 57 (from protein Hydroxymethylglutaryl-CoA lyase) and 127 (from Glycine cleavage system H protein) that show abundant, but opposing trends in liver and brown adipose tissues and yet appear absent or less abundant in other tissues. Global measurements on protein levels including the substrates for acetylation identified here will enable determination of the extent of differential protein acetylation that exists in each tissue. Nonetheless, measurements on protein acetylation patterns themselves may be important for improved understanding of tissues-specific energy sensing mechanisms and energy homeostasis.

4. Comparison of mouse metabolic acetylome under different feeding conditions

Changes of the observed levels of acetylated peptides under fasting and re-feeding conditions are visualized by plotting the $\log_{10}$ (re-fed/fasted) values of the areas of the acetylated peptides in Figure 4. The same acetylated peptides from those metabolic and chaperone proteins plotted in Figure 3 are used in generating Figure 4. The sequences and protein origins of these peptides are listed in Table 1, and their index values are used as the x-axis in Figure 4. For an identified acetylated peptide in a specific tissue, the quantified EIC area from the re-fed sample was divided by that from the fasted sample. Log_{10} (re-fed/fasted) higher than or lower than 0 indicates the acetylated peptide abundance is increased or decreased in the re-fed sample, respectively. Similar to Figure 3, the peptides from the same protein are grouped and shaded to allow visualization of multiple sites for each protein. Furthermore, to determine which acetylated peptides appeared with the highest altered abundance levels, measurements on the distributions of the $\log_{10}$ (re-fed/fasted) data were performed. For each tissue or organ, data from all the quantified peptides were used to plot the distribution of the $\log_{10}$ values. For example, Figure 5 illustrates the distribution derived from the liver data. Most $\log_{10}$ (re-fed/fasted) values are clustered at 0.027 (approximately 1:1 of re-fed: fasted), only a few are distant from the distribution center. The average and standard deviation were then calculated from the distribution plot. Acetylated peptides with ratios greater than ± two standard deviations from the mean were selected as those with the top 5% largest changed levels (> 3-fold change, more discussion in the supplementary file).

In this way, a total of 58 acetylated peptides were found to show the greatest altered levels under fasted/re-feeding conditions (> 3-fold change) from seven tissues or organs, among which 31 peptides are from the 23 selected metabolic proteins and chaperones (listed in Table 2 and marked with * in Figure 4). Excitingly, many of the $\log_{10}$ (re-fed/fasted) values for insulin sensitive tissues, such as liver, brown adipose and skeletal muscle are negative, which indicates acetylation levels for a majority of proteins are decreased in these tissues under the re-feeding condition. On the other hand, insulin insensitive organs like kidney and brain show the opposite trend and the $\log_{10}$ (re-fed/fasted) values of many proteins are observed to be positive. This suggests that re-fed/fasted acetylation changes reflect tissue-specific fuel utilization changes (metabolic flexibility), rather than being an indicator of tissue or organ specific insulin effects. For example, if insulin-specific effects were the only cause for the shift in acetylation patterns between fasted and re-fed conditions, one might expect that insulin insensitive organs to exhibit little or no change upon re-feeding. The altered abundance levels of the acetylated peptides may be resultant from the altered acetylation levels in the fasted and re-fed mice, and/or altered protein levels. To investigate this, catalase and alcohol dehydrogenase protein levels in fasted and re-fed mouse liver samples were measured with western blot analyses (Supplementary Figure 3). The quantification results show that the protein levels are unaltered, while the acetylation levels detected on peptides from these proteins appear with fasted-to-fed ratios among the top 5% of all those measured (greater than 3-fold change). In addition, it should be noted that differential regulation of these proteins on a tissue-specific basis, whether that includes PTM levels, protein abundance levels or both implicates differing functional role of these species in each tissue under different feeding conditions. This in itself presents a novel and exciting result that can impact understanding of metabolic regulation in a new way. Furthermore in several cases, many peptides from a given protein were identified as acetylated; however only one or a couple were found to change more than 3-fold. For example, 2–10 acetylated peptides were quantified from protein G (ATP synthase F_6) from each tissue or organ; however the re-fed/fasted ratios for most peptides hover around 1:1 in all the cases except for peptide 25 in skeletal muscle. Another example is protein I (creatine kinase M-type). In this case, the difference between muscle and the other tissues is dramatic. In skeletal and heart muscle, more than 10 acetylated peptides of creatine kinase were quantified; however none of those peptides could be quantified in any of the other tissues. Such observation illustrates excellent agreement with the known tissue-specific expression since this protein is found with expression in skeletal muscle much higher than in any other tissue and agrees with the finding of creatine kinase M acetylation in an earlier report[25]. On the peptide level, from the 19 quantified acetylated peptides from creatine kinase M-type in skeletal muscle, the level changes of only 2 were found to change greater than 3-fold, while the other 17 appear unchanged. Such observation highlights the significance of acetylation on those two specific sites. In another case, different subunits of a complex were acetylated in different tissues. For example, the F_6 subunit of the peripheral arm of the ATP synthase complex[49] was hyperacetylated in skeletal muscle, whereas the oligomycin sensitivity conferral protein (OSCP) of the peripheral arm was hyperacetylated in kidney, but hypoacetylated in liver. Further investigations of three-dimensional structures of these acetylated lysine sites may reveal key mechanisms relevant to protein function and how they can be modulated by acetylation under different physiological conditions.

Figure 6 shows the proteins with greater than 3-fold differences in acetylation between the fasted and re-fed states in the context of metabolism, including fatty acid oxidation, glycolysis, the citric acid cycle and oxidative phosphorylation. Table 3 also shows that there were organ specific differences in these proteins with the biggest number of proteins detected in kidney, brown adipose and liver. From Table 3 and Figure 6 it appears that many of the enzymes with differences in the abundance of acetylated peptides between the fasted and re-fed state are involved in the production of acetyl CoA or its consumption in the TCA

cycle and oxidative phosphorylation. The majority of the metabolic proteins with differences in the abundance of acetylated peptides are detected in one organ only. The exceptions are the OSCP of F_oF_1-ATP synthase (kidney and liver) and hydroxymethylglutaryl-CoA lyase (HMGCL) (kidney and brown adipose), and the mitochondrial voltage dependent anion channel 1 (mVDAC1) (liver and heart).

Discussion

Approximately 2000 acetylated proteins have been previously identified in mammalian cells, and metabolic enzymes are highly represented[7, 9, 30, 31]. It has been postulated, mainly on the basis of liver proteomic studies, that acetylation serves to coordinate flux in the central metabolism network, as nearly all enzymes involved in glycolysis, gluconeogenesis, the TCA cycle, fatty acid oxidation, the urea cycle, glycogen metabolism, OXPHOS, and amino acid metabolism are acetylated (reviewed in Guan and Xiong[32], and Patel *et al*[30]). The global tissue and organ specific metabolic acetylome data we have collected, summarized in Table 3 and Figure 6, is more extensive than has been done previously, and suggests something further, that changes in lysine acetylation may control tissue specific fuel switching between the fasted and fed states. Between the fasted and re-fed states, our results showed a large number of proteins with greater than 3-fold differences in the abundance of their acetylated peptides in metabolic pathways of the TCA cycle, β-oxidation, oxidative phosphorylation and glycolysis, as well as associated chaperones and transport proteins. Furthermore, these differences were organ specific, and heavily mitochondrial biased (Table 3), even though our global technique used whole tissue and did not enrich for mitochondria (Figure 1). Lysine acetylation has been associated with increases or decreases in protein activity[9,31–33], and it will require metabolomic and fluxomic profiling to distinguish whether organs showed different metabolic responses to the fasted to re-fed transition that correlated positively or negatively with acetylation. Certainly, studies showing acetylation of malate dehydrogenase (MDH2) increases in response to glucose, and deacetylation of MDH2 decreases its activity[9], support regulation of TCA cycle flux by acetylation in response to glucose changes that can occur with fasting and re-feeding. Considerations of TCA cycle flux regulation will require both metabolic profiling and fluxomic studies as while MDH2 activity is increased by acetylation, deacetylation of the SdhA subunit, key for coupling TCA cycle flux to the OXPHOS chain, increased the Complex II activity[33].

One might speculate on the tissue specific effects of acetylation, based on our fasted/re-fed data (described in Fig. 4). For example, in skeletal muscle, glycolysis and creatine phosphorylation should be more active in the re-fed state[34, 35], where we see decreases of acetylation levels in creatine kinase M-type and fructose-bisphosphate aldolase A. Thus, acetylation may be used to negatively regulate these enzyme activities in times when blood glucose levels drop, decreasing demands for glycolysis and energy storage. On the other hand, the increased re-fed/fasted acetylation of ATP synthase F_6 may facilitate the synthesis of ATP for the fed state. In heart muscle, VDAC1, the voltage-dependent anion-selective channel, is hypoacetylated. VDACs behave as a general diffusion pore for small hydrophilic molecules, with a voltage-dependent switch between an anion-selective high-conductance state with high metabolite flux and a cation-selective low-conductance state with limited passage of metabolites. It may be that acetylation restricts the passage of metabolites, which would be increased for the fasted to fed transition. Heart MDH2 is hyperacetylated, in agreement with the increased TCA cycle flux expected for the fed *vs*. fasted state. For liver, the decreased re-fed/fasted acetylation for cytochrome c oxidase subunit 4, ATP synthase OSCP subunit, VDAC1, enoyl CoA hydratase 1 (ECH1), and alcohol dehydrogenase (ADH) may all serve to maximize fuel storage, and energy generation in the fasted to fed transition. As shown in Figure 6, ECH1 activity is key to unsaturated fatty acid oxidation, and it is

known that acetylation increases the activity of another enzyme of fatty acid oxidation, enoyl-coenzyme A hydratase/3-hydroxyacyl-coenzyme A (EHHADH)[9]. Therefore, in the fed state, where fatty acid synthesis is active, it is logical that ECH1 is hypoacetylated, with presumably decreased activity. ADH may help funnel glycerol (increased from hydrolysis of triglycerides in the intestine after re-feeding) into the glycolytic pathway (Figure 6), and presumably hypoacetylation would increase ADH activity. Detailed discussion on the acetylation changes in many other proteins in different organs or tissues are included in the supplementary discussion. It is important to note however, that altered levels of acetylated peptides identified here include both biologically-significant level changes and those due to normal biological variation. Thus while not conclusive, the acetylation sites identified in this manuscript serve as useful guide for further biological studies and for the first time, show the variability in acetylation site levels that exists within different tissues from the same animals.

Conclusion

Lysine acetylation is emerging as a critical PTM found in many areas and may be part of a fasted/re-fed feedback control system for metabolic network regulation fuel switching. Thus, proteome studies are critical to elucidate and help understand the functional roles fulfilled by protein acetylation. This study presents the most comprehensive acetylome data from a set of mouse organs produced to date. Seven hundred and thirty-three acetylated peptides from 337 mouse proteins were identified and quantified, many of which are likely relevant to fasted/re-fed transition and fuel switching. From this comprehensive acetylome dataset, a new view is attained revealing previously unrecognized differential acetylation that is present in various organs or tissues derived from the same set of animals. Different organs such as liver, brown and white adipose, skeletal and heart muscle, kidney and brain show dramatic variation in quantitative profiles of acetylated peptides under differential feeding conditions. A total of 58 acetylated peptides changed 3-fold or greater under fasted/re-fed conditions, 31 of which are from metabolic proteins or chaperones. These acetylated sites represent a valuable set of targets to guide future research on fuel switching and molecular pathways relevant to metabolic disorders.

Supplementary Material

Refer to Web version on PubMed Central for supplementary material.

Acknowledgments

We thank Professor Derek LeRoith from Metabolism Institute, Mount Sinai Medical Centre for providing the FVB/N mice used. The present work was supported by NIH grants R01GM086688, R01RR023334 and S10RR025107 to J. E. Bruce; DK58132-01A2 grant to I. J. Kurland, and method development is additionally supported by Diabetes Research and Training Center (DRTC) NIH grant P60DK020541, and NIAID grant U19AI091175-01. A. J. Robinson is supported by the Medical Research Council, UK. Supporting Information Available: This material is available free of charge via the Internet at http://pubs.acs.org.

References

1. Batta K, Das C, Gadad S, Shandilya J, Kundu TK. Reversible acetylation of non histone proteins: role in cellular function and disease. Subcell Biochem. 2007; 41:193–212. [PubMed: 17484129]
2. Spange S, Wagner T, Heinzel T, Kramer OH. Acetylation of non-histone proteins modulates cellular signalling at multiple levels. Int J Biochem Cell Biol. 2009; 41(1):185–98. [PubMed: 18804549]
3. Norris KL, Lee JY, Yao TP. Acetylation goes global: the emergence of acetylation biology. Sci Signal. 2009; 2(97):pe76. [PubMed: 19920250]

4. Kouzarides T. Acetylation: a regulatory modification to rival phosphorylation? Embo J. 2000; 19(6): 1176–9. [PubMed: 10716917]
5. Yang XJ. The diverse superfamily of lysine acetyltransferases and their roles in leukemia and other diseases. Nucleic Acids Res. 2004; 32(3):959–76. [PubMed: 14960713]
6. Mischerikow N, Heck AJ. Targeted large-scale analysis of protein acetylation. Proteomics. 2011; 11(4):571–89. [PubMed: 21246731]
7. Choudhary C, Kumar C, Gnad F, Nielsen ML, Rehman M, Walther TC, Olsen JV, Mann M. Lysine acetylation targets protein complexes and co-regulates major cellular functions. Science. 2009; 325(5942):834–40. [PubMed: 19608861]
8. Kim SC, Sprung R, Chen Y, Xu Y, Ball H, Pei J, Cheng T, Kho Y, Xiao H, Xiao L, Grishin NV, White M, Yang XJ, Zhao Y. Substrate and functional diversity of lysine acetylation revealed by a proteomics survey. Mol Cell. 2006; 23(4):607–18. [PubMed: 16916647]
9. Zhao S, Xu W, Jiang W, Yu W, Lin Y, Zhang T, Yao J, Zhou L, Zeng Y, Li H, Li Y, Shi J, An W, Hancock SM, He F, Qin L, Chin J, Yang P, Chen X, Lei Q, Xiong Y, Guan KL. Regulation of cellular metabolism by protein lysine acetylation. Science. 2010; 327(5968):1000–4. [PubMed: 20167786]
10. Kendrick AA, Choudhury M, Rahman SM, McCurdy CE, Friederich M, Van Hove JL, Watson PA, Birdsey N, Bao J, Gius D, Sack MN, Jing E, Kahn CR, Friedman JE, Jonscher KR. Fatty liver is associated with reduced SIRT3 activity and mitochondrial protein hyperacetylation. Biochem J. 2011; 433(3):505–14. [PubMed: 21044047]
11. Schwer B, Eckersdorff M, Li Y, Silva JC, Fermin D, Kurtev MV, Giallourakis C, Comb MJ, Alt FW, Lombard DB. Calorie restriction alters mitochondrial protein acetylation. Aging Cell. 2009; 8(5):604–6. [PubMed: 19594485]
12. McClatchy DB, Liao L, Park SK, Xu T, Lu B, Yates Iii JR. Differential proteomic analysis of mammalian tissues using SILAM. PLoS One. 2011; 6(1):e16039. [PubMed: 21283754]
13. Storlien LH, Baur LA, Kriketos AD, Pan DA, Cooney GJ, Jenkins AB, Calvert GD, Campbell LV. Dietary fats and insulin action. Diabetologia. 1996; 39(6):621–31. [PubMed: 8781757]
14. Chomentowski P, Coen PM, Radikova Z, Goodpaster BH, Toledo FG. Skeletal muscle mitochondria in insulin resistance: differences in intermyofibrillar versus subsarcolemmal subpopulations and relationship to metabolic flexibility. J Clin Endocrinol Metab. 2011; 96(2): 494–503. [PubMed: 21106709]
15. Galgani JE, Moro C, Ravussin E. Metabolic flexibility and insulin resistance. Am J Physiol Endocrinol Metab. 2008; 295(5):E1009–17. [PubMed: 18765680]
16. Kelley DE, Mandarino LJ. Fuel selection in human skeletal muscle in insulin resistance: a reexamination. Diabetes. 2000; 49(5):677–83. [PubMed: 10905472]
17. Mandarino LJ, Consoli A, Jain A, Kelley DE. Interaction of carbohydrate and fat fuels in human skeletal muscle: impact of obesity and NIDDM. Am J Physiol. 1996; 270(3 Pt 1):E463–70. [PubMed: 8638694]
18. Storlien L, Oakes ND, Kelley DE. Metabolic flexibility. Proc Nutr Soc. 2004; 63(2):363–8. [PubMed: 15294056]
19. Rolfe DF, Brown GC. Cellular energy utilization and molecular origin of standard metabolic rate in mammals. Physiol Rev. 1997; 77(3):731–58. [PubMed: 9234964]
20. Blaxter, K. Energy metabolism in animals and man. Cambridge University Press; 1989.
21. Cannon B, Nedergaard J. Metabolic consequences of the presence or absence of the thermogenic capacity of brown adipose tissue in mice (and probably in humans). Int J Obes (Lond). 2010; 34 (Suppl 1):S7–16. [PubMed: 20935668]
22. Bartelt A, Bruns OT, Reimer R, Hohenberg H, Ittrich H, Peldschus K, Kaul MG, Tromsdorf UI, Weller H, Waurisch C, Eychmuller A, Gordts PL, Rinninger F, Bruegelmann K, Freund B, Nielsen P, Merkel M, Heeren J. Brown adipose tissue activity controls triglyceride clearance. Nat Med. 2011; 17(2):200–5. [PubMed: 21258337]
23. Yang L, Zhang H, Bruce JE. Optimizing the detergent concentration conditions for immunoprecipitation (IP) coupled with LC-MS/MS identification of interacting proteins. Analyst. 2009; 134(4):755–62. [PubMed: 19305927]

24. Weisbrod CR, Hoopmann MR, Senko MW, Bruce JE. A New Dual Linear Ion Trap Fourier Transform Ion Cyclotron Resonance Mass Spectrometer: the Velos-FT. Anal Chem. 2011 Submitted 12/10.
25. Iwabata H, Yoshida M, Komatsu Y. Proteomic analysis of organ-specific post-translational lysine-acetylation and -methylation in mice by use of anti-acetyllysine and -methyllysine mouse monoclonal antibodies. Proteomics. 2005; 5(18):4653–64. [PubMed: 16247734]
26. Hoopmann MR, Finney GL, MacCoss MJ. High-speed data reduction, feature detection, and MS/MS spectrum quality assessment of shotgun proteomics data sets using high-resolution mass spectrometry. Anal Chem. 2007; 79(15):5620–32. [PubMed: 17580982]
27. Jonas A, Weber G. Presence of arginine residues at the strong, hydrophobic anion binding sites of bovine serum albumin. Biochemistry. 1971; 10(8):1335–9. [PubMed: 5103997]
28. Lipton MS, Pasa-Tolic L, Anderson GA, Anderson DJ, Auberry DL, Battista JR, Daly MJ, Fredrickson J, Hixson KK, Kostandarithes H, Masselon C, Markillie LM, Moore RJ, Romine MF, Shen Y, Stritmatter E, Tolic N, Udseth HR, Venkateswaran A, Wong KK, Zhao R, Smith RD. Global analysis of the Deinococcus radiodurans proteome by using accurate mass tags. Proc Natl Acad Sci U S A. 2002; 99(17):11049–54. [PubMed: 12177431]
29. Cox J, Mann M. MaxQuant enables high peptide identification rates, individualized p.p.b-range mass accuracies and proteome-wide protein quantification. Nat Biotechnol. 2008; 26(12):1367–72. [PubMed: 19029910]
30. Patel J, Pathak RR, Mujtaba S. The biology of lysine acetylation integrates transcriptional programming and metabolism. Nutr Metab (Lond). 2011; 8:12. [PubMed: 21371315]
31. Yao YL, Yang WM. Beyond histone and deacetylase: an overview of cytoplasmic histone deacetylases and their nonhistone substrates. J Biomed Biotechnol. 2011; 2011:146493. [PubMed: 21234400]
32. Guan KL, Xiong Y. Regulation of intermediary metabolism by protein acetylation. Trends Biochem Sci. 2011; 36(2):108–16. [PubMed: 20934340]
33. Cimen H, Han MJ, Yang Y, Tong Q, Koc H, Koc EC. Regulation of succinate dehydrogenase activity by SIRT3 in mammalian mitochondria. Biochemistry. 2010; 49(2):304–11. [PubMed: 20000467]
34. Halias HM, Snittyns'kyi VV, Ianovych VH. The regulatory characteristics of creatine kinase activity in the skeletal muscle of piglets in the neonatal period. Fiziol Zh. 1995; 41(1–2):25–9. [PubMed: 8846323]
35. Dumas JF, Bielicki G, Renou JP, Roussel D, Ducluzeau PH, Malthiery Y, Simard G, Ritz P. Dexamethasone impairs muscle energetics, studied by (31)P NMR, in rats. Diabetologia. 2005; 48(2):328–35. [PubMed: 15645207]
36. Wang SP, Robert MF, Gibson KM, Wanders RJ, Mitchell GA. 3-Hydroxy-3-methylglutaryl CoA lyase (HL): mouse and human HL gene (HMGCL) cloning and detection of large gene deletions in two unrelated HL-deficient patients. Genomics. 1996; 33(1):99–104. [PubMed: 8617516]
37. Ross BD, Espinal J, Silva P. Glucose metabolism in renal tubular function. Kidney Int. 1986; 29(1):54–67. [PubMed: 3515015]
38. Cabiscol E, Belli G, Tamarit J, Echave P, Herrero E, Ros J. Mitochondrial Hsp60, resistance to oxidative stress, and the labile iron pool are closely connected in *Saccharomyces cerevisiae*. J Biol Chem. 2002; 277(46):44531–8. [PubMed: 12200437]
39. Shan Y, Napoli E, Cortopassi G. Mitochondrial frataxin interacts with ISD11 of the NFS1/ISCU complex and multiple mitochondrial chaperones. Hum Mol Genet. 2007; 16(8):929–41. [PubMed: 17331979]
40. Tsai CL, Barondeau DP. Human frataxin is an allosteric switch that activates the Fe-S cluster biosynthetic complex. Biochemistry. 2010; 49(43):9132–9. [PubMed: 20873749]
41. Rouault TA, Tong WH. Iron-sulfur cluster biogenesis and human disease. Trends Genet. 2008; 24(8):398–407. [PubMed: 18606475]
42. Scroggins BT, Robzyk K, Wang D, Marcu MG, Tsutsumi S, Beebe K, Cotter RJ, Felts S, Toft D, Karnitz L, Rosen N, Neckers L. An acetylation site in the middle domain of Hsp90 regulates chaperone function. Mol Cell. 2007; 25(1):151–9. [PubMed: 17218278]

43. Wang Y, Wang SY, Zhang XH, Zhao M, Hou CM, Xu YJ, Du ZY, Yu XD. FK228 inhibits Hsp90 chaperone function in K562 cells via hyperacetylation of Hsp70. Biochem Biophys Res Commun. 2007; 356(4):998–1003. [PubMed: 17397803]
44. Perkins DN, Pappin DJ, Creasy DM, Cottrell JS. Probability-based protein identification by searching sequence databases using mass spectrometry data. Electrophoresis. 1999; 20(18):3551–3567. [PubMed: 10612281]
45. Elias JE, Haas W, Faherty BK, Gygi SP. Comparative evaluation of mass spectrometry platforms used in large-scale proteomics investigations. Nat Methods. 2005; 2(9):667–675. [PubMed: 16118637]
46. Karp NA, Lilley KS. Investigating sample pooling strategies for DIGE experiments to address biological variability. Proteomics. 2009; 9(2):388–397. [PubMed: 19105178]
47. Kendziorski C, Irizarry RA, Chen KS, Haag JD, Gould MN. On the utility of pooling biological samples in microarray experiments. Proc Natl Acad Sci U S A. 2005; 102(12):4252–4257. [PubMed: 15755808]
48. Diz AP, Truebano M, Skibinski DO. The consequences of sample pooling in proteomics: an empirical study. Electrophoresis. 2009; 30(17):2967–2975. [PubMed: 19676090]
49. Rees DM, Leslie AG, Walker JE. The structure of the membrane extrinsic region of bovine ATP synthase. Proc Natl Acad Sci U S A. 2009; 106(51):21597–21601. [PubMed: 19995987]

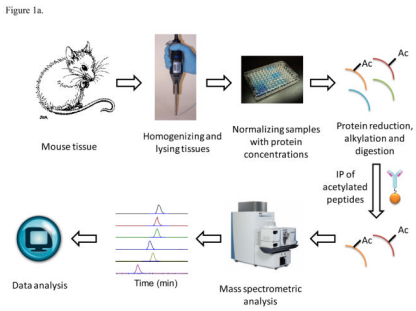

Figure 1b

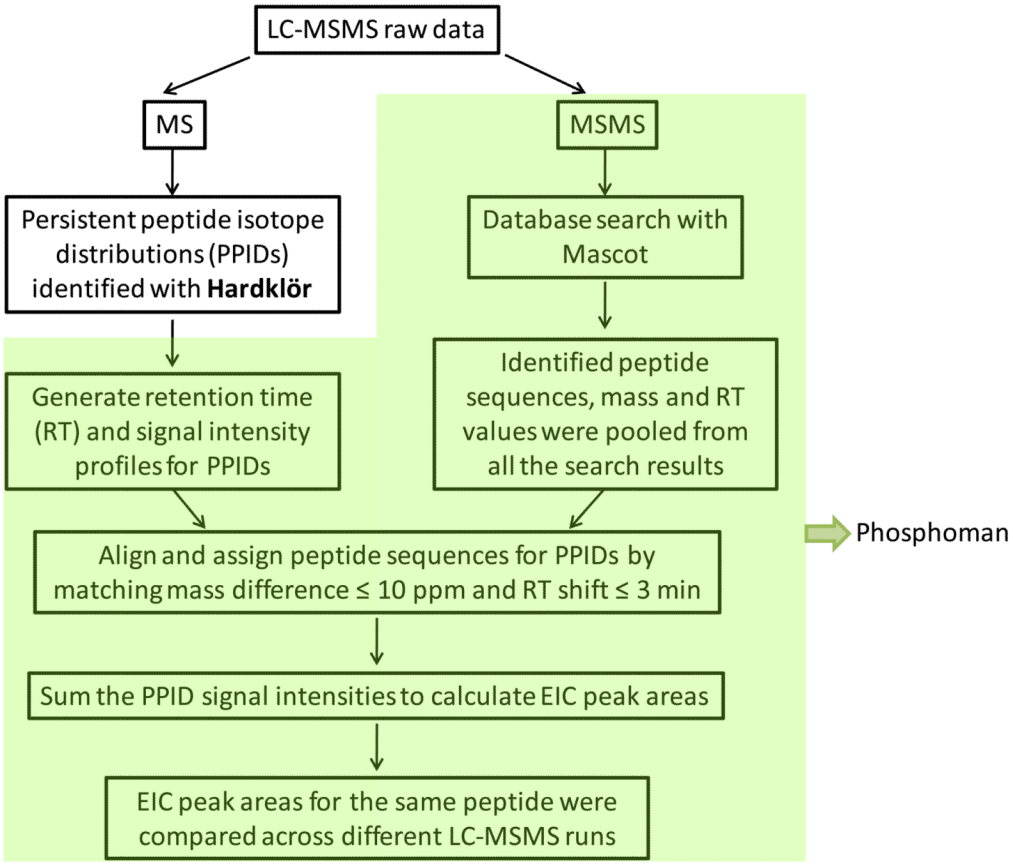

Figure 1.

Experimental Scheme. Seven tissues or organs from the same 5 fasted or re-fed mice were pooled, homogenized and lysed. Different samples were normalized using the same starting amount of total protein. Thirty milligrams of protein from each sample were reduced and alkylated, trypsin digested, and anti-acetylated lysine antibody beads were used for immunoprecipitation from the digested protein sample supernatants. The enriched acetylation products were fractionated with UPLC (nanoAcquity Waters, Milford, MA) and analyzed with a built-in-house Velos-FT mass spectrometer[24] (see Methods).

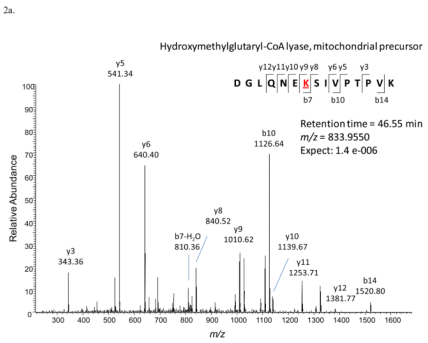

Figure 2b.

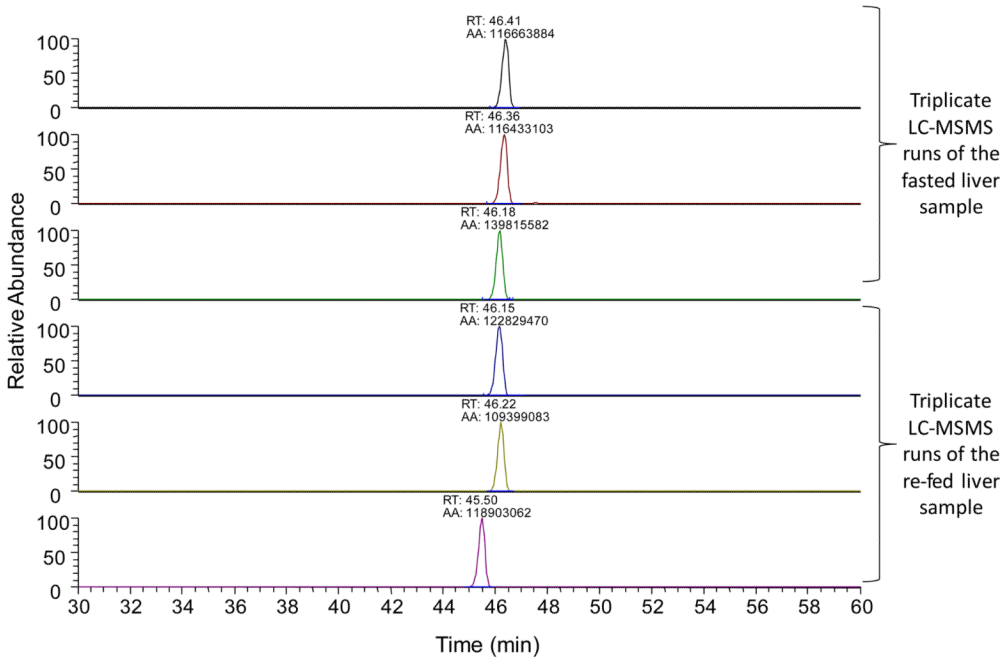

Figure 2c.

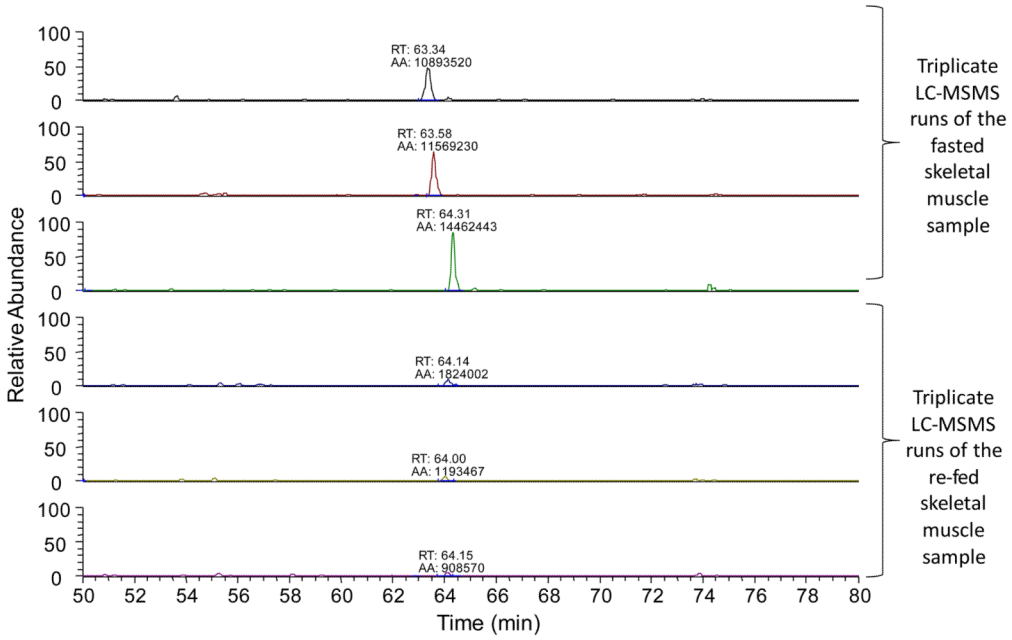

Figure 2.

An example of LFQ analysis of the acetylated peptides

2a. Identification of the acetylated peptide DGLQNEK@SIVPTPVK with the LC-MSMS data and Mascot database search. The modified lysine residue is marked with @.

2b. EIC peaks of the acetylated peptide DGLQNEK@SIVPTPVK with the retention time and peak areas labeled. The retention time shift is less than 1 min. The peak areas are used in the LFQ analysis.

2c. An example of a peptide with altered abundance observed during fasted-to-fed transition: FCVGLQK@IEEIFKK.

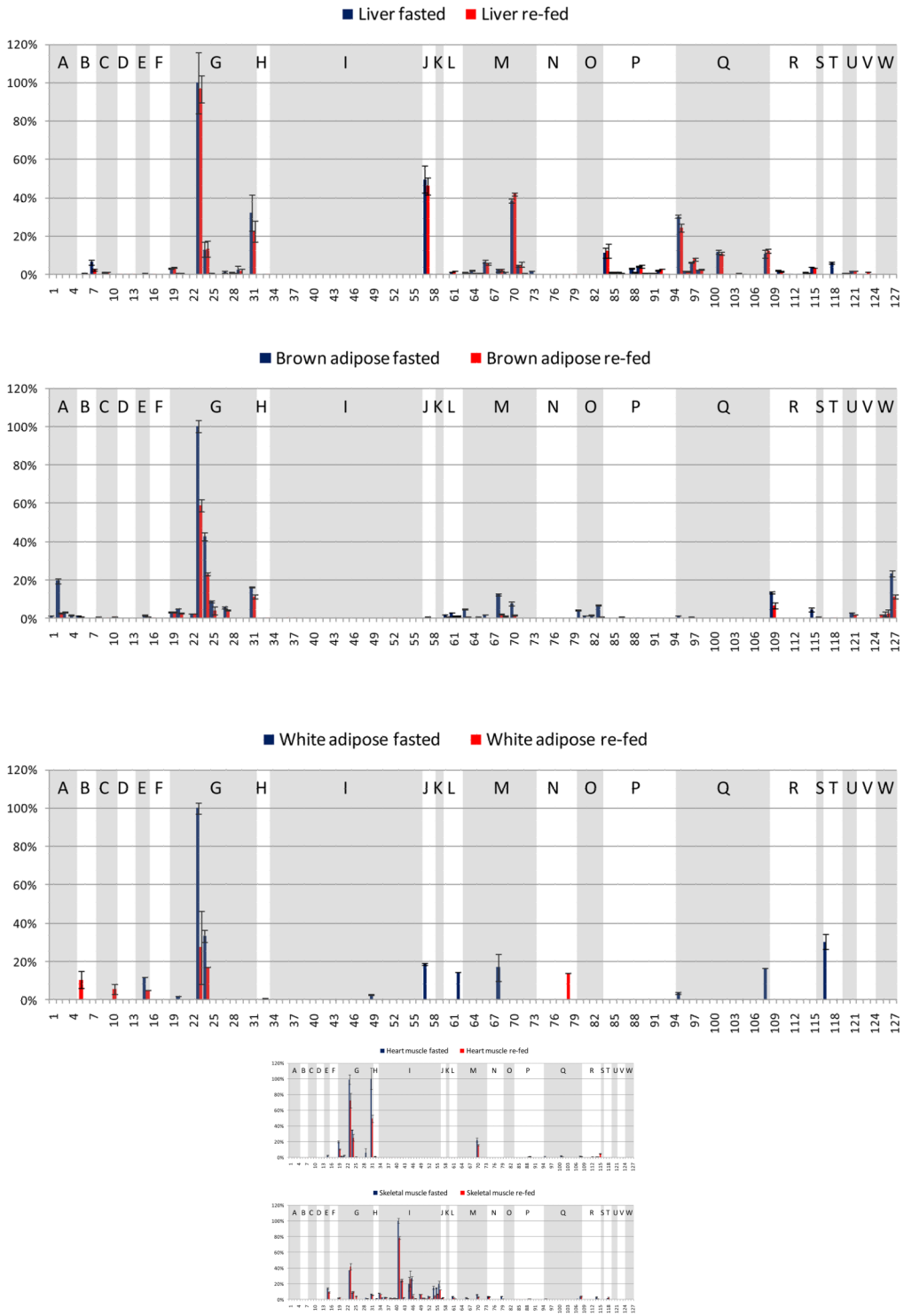

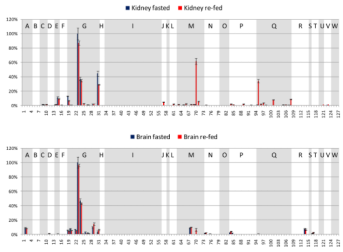

Figure 3.

Fasted and re-fed tissue-specific mouse acetylome profiles of the selected 127 acetylated peptides from the 23 metabolic proteins and chaperones. x-axis: the index number of the selected 127 acetylated peptides, y-axis: relative EIC area (the EIC area of a specific acetylated peptide divided by that of the most abundant acetylated peptide from the selected proteins in that tissue). Blue bars indicate the fasted state, pink bars the re-fed state. Shown panels are: a. liver, b. brown adipose, c. white adipose, d. heart muscle, e. skeletal muscle, f. kidney, g. brain. The peptides from the same protein are grouped, and the proteins are indicated with single letters.

A: Aconitate hydratase, mitochondrial precursor (ACO2)
B: Cytochrome c oxidase subunit 4 isoform 1, mitochondrial precursor (COX4)
C: Cytochrome b5 type B precursor (Cyb5b)
D: Electron transfer flavoprotein subunit beta (β-ETF)
E: Isoform Pl-VDAC1 of Voltage-dependent anion-selective channel protein 1 (VDAC1)
F: ATP synthase O subunit, mitochondrial precursor (OSCP)
G: ATP synthase coupling factor 6, mitochondrial precursor (F6)
H: Creatine kinase, sarcomeric mitochondrial precursor (S-MtCK)
I: Creatine kinase M-type (M-CK)
J: Hydroxymethylglutaryl-CoA lyase, mitochondrial precursor (HMGCL)
K: Product of the ECH1 gene, Delta(3,5)-Delta(2,4)-dienoyl-CoA isomerase, mitochondrial precursor (ECH1)
L: Dihydrolipoyllysine-residue succinyltransferase component of 2-oxoglutarate dehydrogenase complex, mitochondrial precursor (α-KGDH)
M: Acetyl-CoA acetyltransferase, mitochondrial precursor (ACAT1)
N: Fructose-bisphosphate aldolase A (ALDOA)
O: Hydroxyacyl-Coenzyme A dehydrogenase/3-ketoacyl-Coenzyme A thiolase/enoyl-Coenzyme A hydratase (Trifunctional protein), alpha subunit (TP-α)
P: L: Stress-70 protein, mitochondrial precursor (GRP-75)
Q: 60 kDa heat shock protein, mitochondrial precursor (HSP-60)
R: Malate dehydrogenase, mitochondrial precursor (MDH2)
S: Propionyl-CoA carboxylase alpha chain, mitochondrial precursor (PCCA-α)
T: Alcohol dehydrogenase (ADH)
U: D-dopachrome decarboxylase (DDT)
V: Catalase (CAT)
W: Glycine cleavage system H protein, mitochondrial precursor (GCSH)

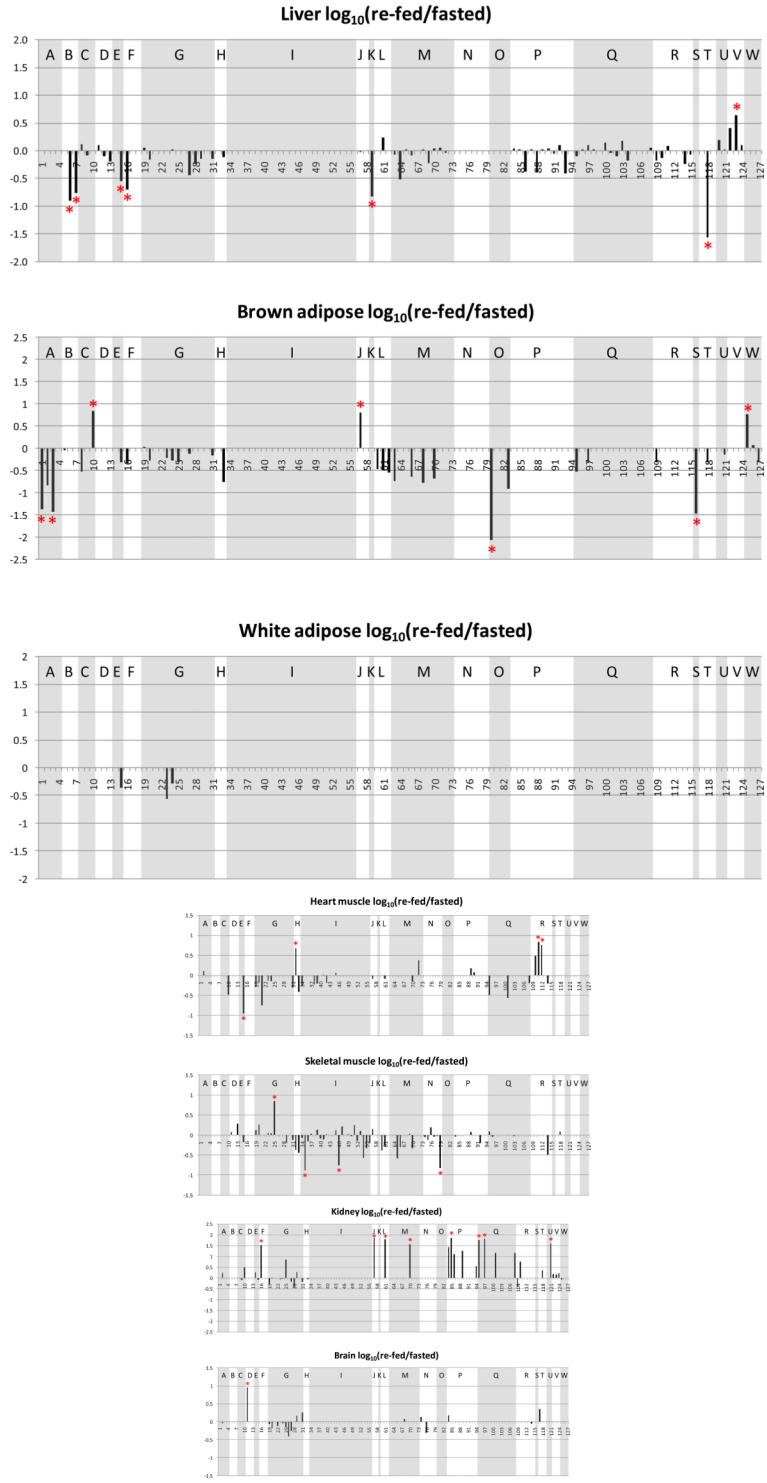

Figure 4.

Log_{10} (re-fed/fasted) values of the acetylated peptide EIC areas in different tissues. Shown panels are: a. liver, b. brown adipose, c. white adipose, d. heart muscle, e. skeletal muscle, f. kidney, g. brain. The peptides from the same protein are grouped, and the proteins are indicated the same as in Figure 3.

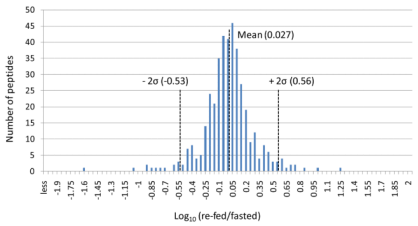

Figure 5.

Distribution plot of the liver $\log_{10}$ (re-fed/fasted) data. The center of the distribution is 0.027, and the standard deviation is 0.267.

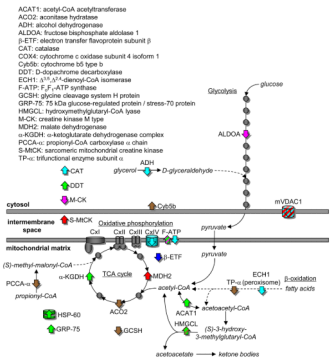

Figure 6.

Differences in tissue-specific acetylation of enzymes, transporters and chaperones of bioenergetic pathways in the cytoplasm and mitchondrial matrix between fasted and re-fed mice. Proteins showing a re-fed:fasted ratios of the extracted ion chromatographic peak areas for the persistent peptide isotope distributions greater than 3 are shown as an up arrow (⇑) and less than 0.33 as a down arrow (⇓), The proteins are color-coded according to tissue: brain (blue), brown fat (brown), heart muscle (red), kidney (green), liver (cyan) and skeletal muscle (magenta). Proteins showing no differential acetylation are shown as grey circles.

Table 1

Identified acetylated peptides from the selected metabolic and chaperone proteins

Index	Protein accession number	Protein name	Peptide sequence
1	IPI00116074	Aconitate hydratase, mitochondrial precursor	AIITK@SFAR
2	IPI00116074	Aconitate hydratase, mitochondrial precursor	YDLLEK@NINIVR
3	IPI00116074	Aconitate hydratase, mitochondrial precursor	FK@LEAPDADELPR
4	IPI00116074	Aconitate hydratase, mitochondrial precursor	CTTDHISAAGPWLK@FR
5	IPI00117978	Cytochrome c oxidase subunit 4 isoform 1, mitochondrial precursor	WDYDK@NEWK
6	IPI00117978	Cytochrome c oxidase subunit 4 isoform 1, mitochondrial precursor	AHGSVVK@SEDYAFPTYADR
7	IPI00117978	Cytochrome c oxidase subunit 4 isoform 1, mitochondrial precursor	AHGSVVK@SEDYAFPTYADRR
8	IPI00315794	Cytochrome b5 type B precursor	QYYIGDVHPSDLK@PK
9	IPI00315794	Cytochrome b5 type B precursor	EM#LK@QYYIGDVHPSDLKPK
10	IPI00315794	Cytochrome b5 type B precursor	ATPEASGSGEK@VEGSEPSVTYYR
11	IPI00121440	Electron transfer flavoprotein subunit beta	VLAK@LAEK
12	IPI00121440	Electron transfer flavoprotein subunit beta	VLAK@LAEKEK
13	IPI00121440	Electron transfer flavoprotein subunit beta	LAEKEK@VDLLFLGK
14	IPI00122549	Isoform Pl-VDAC1 of Voltage-dependent anion-selective channel protein 1	LTLSALLDGK@NVNAGGHK
15	IPI00122549	Isoform Pl-VDAC1 of Voltage-dependent anion-selective channel protein 1	FGIAAK@YQVDPDACFSAK
16	IPI00118986	ATP synthase O subunit, mitochondrial precursor	IGEK@YVDMSAK
17	IPI00118986	ATP synthase O subunit, mitochondrial precursor	TVKVK@SLNDITK
18	IPI00118986	ATP synthase O subunit, mitochondrial precursor	TVK@VKSLNDITK
19	IPI00125460	ATP synthase coupling factor 6, mitochondrial precursor	LFVDK@IR
20	IPI00125460	ATP synthase coupling factor 6, mitochondrial precursor	FEVIDK@PQS
21	IPI00125460	ATP synthase coupling factor 6, mitochondrial precursor	LFVDK@IREYK
22	IPI00125460	ATP synthase coupling factor 6, mitochondrial precursor	ELDPVQK@LFVDK
23	IPI00125460	ATP synthase coupling factor 6, mitochondrial precursor	FDDPKFEVIDK@PQS
24	IPI00125460	ATP synthase coupling factor 6, mitochondrial precursor	FDDPK@FEVIDKPQS
25	IPI00125460	ATP synthase coupling factor 6, mitochondrial precursor	FDDPK@FEVIDK@PQS
26	IPI00125460	ATP synthase coupling factor 6, mitochondrial precursor	GEMDTFPTFK@FDDPK
27	IPI00125460	ATP synthase coupling factor 6, mitochondrial precursor	GEM#DTFPTFK@FDDPK
28	IPI00125460	ATP synthase coupling factor 6, mitochondrial precursor	QM#YGK@GEM#DTFPTFK
29	IPI00125460	ATP synthase coupling factor 6, mitochondrial precursor	GEMDTFPTFKFDDPK@FEVIDKPQS

Index	Protein accession number	Protein name	Peptide sequence
30	IPI00125460	ATP synthase coupling factor 6, mitochondrial precursor	GEMDTFPTFK@FDDPKFEVIDKPQS
31	IPI00125460	ATP synthase coupling factor 6, mitochondrial precursor	GEMDTFPTFKFDDPK@FEVIDKPQS
32	IPI00120076	Creatine kinase, sarcomeric mitochondrial precursor	FSK@ILENLR
33	IPI00120076, IPI00127596	Creatine kinase, sarcomeric mitochondrial precursor	VISM#EK@GGNM#K
34	IPI00127596	Creatine kinase M-type	GK@YYPLK
35	IPI00127596	Creatine kinase M-type	IEEIFK@K
36	IPI00127596	Creatine kinase M-type	HGGYK@PTDK
37	IPI00127596	Creatine kinase M-type	LANLSK@HPK
38	IPI00127596	Creatine kinase M-type	LM#VEM#EK@K
39	IPI00127596	Creatine kinase M-type	PFGNTHNK@FK
40	IPI00127596	Creatine kinase M-type	GGVHVK@LANLSK
41	IPI00127596	Creatine kinase M-type	HPK@FEEILTR
42	IPI00127596	Creatine kinase M-type	VLTPDLYNK@LR
43	IPI00127596	Creatine kinase M-type	FCVGLQK@IEEIFK
44	IPI00127596	Creatine kinase M-type	LSVEALNSLTGEFK@GK
45	IPI00127596	Creatine kinase M-type	LNYK@PQEEYPDLSK
46	IPI00127596	Creatine kinase M-type	FCVGLQK@IEEIFKK
47	IPI00127596	Creatine kinase M-type	HNNHM#AK@VLTPDLYNK
48	IPI00127596	Creatine kinase M-type	AVEK@LSVEALNSLTGEFK
49	IPI00127596	Creatine kinase M-type	FKLNYK@PQEEYPDLSK
50	IPI00127596	Creatine kinase M-type	FK@LNYKPQEEYPDLSK
51	IPI00127596	Creatine kinase M-type	LSVEALNSLTGEFKGK@YYPLK
52	IPI00127596	Creatine kinase M-type	TDLNHENLK@GGDDLDPNYVLSSR
53	IPI00127596	Creatine kinase M-type	HKTDLNHENLK@GGDDLDPNYVLSSR
54	IPI00127596	Creatine kinase M-type	SMTEQEQQQLIDDHFLFDK@PVSPLLLASGMAR
55	IPI00127596, IPI00127596	Creatine kinase M-type	SMTEQEQQQLIDDHFLFDK@PVSPLLLASGM#AR
56	IPI00127596	Creatine kinase M-type	SM#TEQEQQQLIDDHFLFDK@PVSPLLLASGM#AR
57	IPI00127625	Hydroxymethylglutaryl-CoA lyase, mitochondrial precursor	DGLQNEK@SIVPTPVK
58	IPI00127625	Hydroxymethylglutaryl-CoA lyase, mitochondrial precursor	DGLQNEK@SIVPTPVKIR
59	IPI00130804	Delta(3,5)-Delta(2,4)-dienoyl-CoA isomerase, mitochondrial precursor	SITFSK@L
60	IPI00134809	Dihydrolipoyllysine-residue succinyltransferase component of 2-oxoglutarate dehydrogenase complex, mitochondrial precursor	HK@DAFLK

Index	Protein accession number	Protein name	Peptide sequence
61	IPI00134809	Dihydrolipoyllysine-residue succinyltransferase component of 2-oxoglutarate dehydrogenase complex, mitochondrial precursor	HKDAFLK@K
62	IPI00134809	Dihydrolipoyllysine-residue succinyltransferase component of 2-oxoglutarate dehydrogenase complex, mitochondrial precursor	HNLK@LGFMSAFVK
63	IPI00154054	Acetyl-CoA acetyltransferase, mitochondrial precursor	VLK@YAGLK
64	IPI00154054	Acetyl-CoA acetyltransferase, mitochondrial precursor	VDFSK@VPK
65	IPI00154054	Acetyl-CoA acetyltransferase, mitochondrial precursor	VLK@YAGLKK
66	IPI00154054	Acetyl-CoA acetyltransferase, mitochondrial precursor	GATPYGGVK@LEDLIVK
67	IPI00154054	Acetyl-CoA acetyltransferase, mitochondrial precursor	GKPDVVVK@EDEEYKR
68	IPI00154054	Acetyl-CoA acetyltransferase, mitochondrial precursor	EAWDAGK@FASEITPITISVK
69	IPI00154054	Acetyl-CoA acetyltransferase, mitochondrial precursor	DGLTDVYNK@IHM#GNCAENTAK
70	IPI00154054	Acetyl-CoA acetyltransferase, mitochondrial precursor	SKEAWDAGK@FASEITPITISVK
71	IPI00154054	Acetyl-CoA acetyltransferase, mitochondrial precursor	GATPYGGVK@LEDLIVKDGLTDVYNK
72	IPI00154054	Acetyl-CoA acetyltransferase, mitochondrial precursor	AGIPK@EEVKEVYM#GNVIQGGEGQAPTR
73	IPI00154054	Acetyl-CoA acetyltransferase, mitochondrial precursor	TVFQK@ENGTITAANASTLNDGAAALVLM#TAEAAQR
74	IPI00221402, IPI00119458, IPI00649880	Fructose-bisphosphate aldolase A	DGADFAK@WR
75	IPI00221402, IPI00133580	Fructose-bisphosphate aldolase A	GILAADESTGSIAK@R
76	IPI00221402	Fructose-bisphosphate aldolase A	K@ELSDIAHR
77	IPI00221402, IPI00649880	Fructose-bisphosphate aldolase A	AAQEEYIK@R
78	IPI00221402, IPI00649880	Fructose-bisphosphate aldolase A	CPLLK@PWALTFSYGR
79	IPI00221402	Fructose-bisphosphate aldolase A	CVLK@IGEHTPSALAIMENANVLAR
80	IPI00223092	Hydroxyacyl-Coenzyme A dehydrogenase/3-ketoacyl-Coenzyme A thiolase/ enoyl-Coenzyme A hydratase (Trifunctional protein), alpha subunit	M#FEK@LEK
81	IPI00223092	Hydroxyacyl-Coenzyme A dehydrogenase/3-ketoacyl-Coenzyme A thiolase/ enoyl-Coenzyme A hydratase (Trifunctional protein), alpha subunit	GQQQVFK@GLNDK
82	IPI00223092	Hydroxyacyl-Coenzyme A dehydrogenase/3-ketoacyl-Coenzyme A thiolase/ enoyl-Coenzyme A hydratase (Trifunctional protein), alpha subunit	DSIFSNLIGQLDYK@GFEK
83	IPI00223092	Hydroxyacyl-Coenzyme A dehydrogenase/3-ketoacyl-Coenzyme A thiolase/ enoyl-Coenzyme A hydratase (Trifunctional protein), alpha subunit	AGLEQGSDAGYLAESQK@FGELALTK
84	IPI00133903	Stress-70 protein, mitochondrial precursor	LK@EEISK
85	IPI00133903	Stress-70 protein, mitochondrial precursor	HIVK@EFKR
86	IPI00133903	Stress-70 protein, mitochondrial precursor	NAEK@YAEEDR
87	IPI00133903	Stress-70 protein, mitochondrial precursor	YDDPEVQK@DTK
88	IPI00133903	Stress-70 protein, mitochondrial precursor	NAEK@YAEEDRR

Index	Protein accession number	Protein name	Peptide sequence
89	IPI00133903	Stress-70 protein, mitochondrial precursor	AQFEGIVTDLIK@R
90	IPI00133903	Stress-70 protein, mitochondrial precursor	RYDDPEVQK@DTK
91	IPI00133903	Stress-70 protein, mitochondrial precursor	QATK@DAGQISGLNVLR
92	IPI00133903	Stress-70 protein, mitochondrial precursor	ETGVDLTK@DNM#ALQR
93	IPI00133903	Stress-70 protein, mitochondrial precursor	YDDPEVQKDTK@NVPFK
94	IPI00133903	Stress-70 protein, mitochondrial precursor	ASNGDAWVEAHGK@LYSPSQIGAFVLM#K
95	IPI00308885	60 kDa heat shock protein, mitochondrial precursor	EGFEK@ISK
96	IPI00308885	60 kDa heat shock protein, mitochondrial precursor	IGIEIIK@R
97	IPI00308885	60 kDa heat shock protein, mitochondrial precursor	SIAK@EGFEK
98	IPI00308885	60 kDa heat shock protein, mitochondrial precursor	SIDLK@DKYK
99	IPI00308885	60 kDa heat shock protein, mitochondrial precursor	SIDLKDK@YK
100	IPI00308885	60 kDa heat shock protein, mitochondrial precursor	LAK@LSDGVAVLK
101	IPI00308885	60 kDa heat shock protein, mitochondrial precursor	SIAKEGFEK@ISK
102	IPI00308885	60 kDa heat shock protein, mitochondrial precursor	GVM#LAVDAVIAELK@K
103	IPI00308885, IPI00308885	60 kDa heat shock protein, mitochondrial precursor	VGGTSDVEVNEKK@DR
104	IPI00308885	60 kDa heat shock protein, mitochondrial precursor	VGEVIVTK@DDAM#LLK
105	IPI00308885	60 kDa heat shock protein, mitochondrial precursor	CIPALDSLK@PANEDQK
106	IPI00308885	60 kDa heat shock protein, mitochondrial precursor	TLNDELEIIEGM#K@FDR
107	IPI00308885	60 kDa heat shock protein, mitochondrial precursor	K@PLVIIAEDVDGEALSTLVLNR
108	IPI00308885	60 kDa heat shock protein, mitochondrial precursor	IQEITEQLDITTSEYEKEK@LNER
109	IPI00323592	Malate dehydrogenase, mitochondrial precursor	GEDFVK@NM#K
110	IPI00323592	Malate dehydrogenase, mitochondrial precursor	KGEDFVK@NM#K
111	IPI00323592	Malate dehydrogenase, mitochondrial precursor	ASIKK@GEDFVK
112	IPI00323592	Malate dehydrogenase, mitochondrial precursor	NLGIGK@ITPFEEK
113	IPI00323592	Malate dehydrogenase, mitochondrial precursor	ANTFVAELK@GLDPAR
114	IPI00323592	Malate dehydrogenase, mitochondrial precursor	ITPFEEK@MIAEAIPELK
115	IPI00323592	Malate dehydrogenase, mitochondrial precursor	ITPFEEK@M#IAEAIPELK
116	IPI00330523	Propionyl-CoA carboxylase alpha chain, mitochondrial precursor	TFDK@ILIANR
117	IPI00466128	Alcohol dehydrogenase	YDSTHYK@ETWK
118	IPI00466128	Alcohol dehydrogenase	GDNPFPK@NADGTVR
119	IPI00466128	Alcohol dehydrogenase	M#PLIGLGTWK@SEPGQVK

Index	Protein accession number	Protein name	Peptide sequence
120	IPI00230034	D-dopachrome decarboxylase	FFPLEAWQIGK@K
121	IPI00230034	D-dopachrome decarboxylase	LCAATATILDK@PEDR
122	IPI00312058	Catalase	DAQLFIQK@K
123	IPI00312058	Catalase	TFYTK@VLNEEER
124	IPI00312058	Catalase	IQALLDK@YNAEKPK
125	IPI00453724	Glycine cleavage system H protein, mitochondrial precursor	MTLSDPSELDELM#SEEAYEK@YVK
126	IPI00453724	Glycine cleavage system H protein, mitochondrial precursor	M#TLSDPSELDELMSEEAYEK@YVK
127	IPI00453724	Glycine cleavage system H protein, mitochondrial precursor	M#TLSDPSELDELM#SEEAYEK@YVK

Table 2

Acetylated peptides from metabolic proteins that appear altered in abundance (3-fold or higher) in fasted-to-fed comparison. Note: acetylated peptides from metabolic proteins in white adipose samples were not observed with altered abundance levels of 3-fold or higher and thus, are not included in this table.

liver				
Protein accession number	**Peptide sequence**	**log10(re-fed/fasted)**	**Index**	**Protein name**
IPI00466128	R.GDNPFPK@NADGTVR.Y	−1.56	118	Alcohol dehydrogenase
IPI00117978	R.AHGSVVK@SEDYAFPTYADR.R	−0.90	6	Cytochrome c oxidase subunit 4 isoform 1, mitochondrial precursor
IPI00130804	K.SITFSK@L.-	−0.82	59	Delta(3,5)-Delta(2,4)-dienoyl-CoA isomerase, mitochondrial precursor
IPI00117978	R.AHGSVVK@SEDYAFPTYADRR.D	−0.76	7	Cytochrome c oxidase subunit 4 isoform 1, mitochondrial precursor
IPI00118986	R.IGEK@YVDM#SAK.S	−0.70	16	ATP synthase O subunit, mitochondrial precursor
IPI00122549	R.FGIAAK@YQVDPDACFSAK.V	−0.55	15	Isoform Pl-VDAC1 of Voltage-dependent anion-selective channel protein 1
IPI00312058	R.TFYTK@VLNEEER.K	0.64	123	Catalase
Brown adipose				
Protein accession number	**Peptide sequence**	**log10(re-fed/fasted)**	**Index**	**Protein name**
IPI00223092	R.M#FEK@LEK.S	−2.08	80	Hydroxyacyl-Coenzyme A dehydrogenase/3-ketoacyl-Coenzyme A thiolase/enoyl-Coenzyme A hydratase (Trifunctional protein), alpha subunit
IPI00330523	K.TFDK@ILIANR.G	−1.47	116	Propionyl-CoA carboxylase alpha chain, mitochondrial precursor
IPI00116074	K.FK@LEAPDADELPR.S	−1.43	3	Aconitate hydratase, mitochondrial precursor
IPI00116074	R.AIITK@SFAR.I	−1.37	1	Aconitate hydratase, mitochondrial precursor
IPI00453724	K.MTLSDPSELDELM#SEEAYEK@YVK.S	0.76	125	Glycine cleavage system H protein, mitochondrial precursor
IPI00127625	R.DGLQNEK@SIVPTPVK.I	0.81	57	Hydroxymethylglutaryl-CoA lyase, mitochondrial precursor
IPI00315794	M.ATPEASGSGEK@VEGSEPSVTYYR.L	0.83	10	Cytochrome b5 type B precursor
Heart muscle				
Protein accession number	**Peptide sequence**	**log10(re-fed/fasted)**	**Index**	**Protein name**
IPI00122549	R.FGIAAK@YQVDPDACFSAK.V	−0.95	15	Isoform Pl-VDAC1 of Voltage-dependent anion-selective channel protein 1
IPI00120076	R.FSK@ILENLR.L	0.68	32	Creatine kinase, sarcomeric mitochondrial precursor
IPI00323592	K.NLGIGK@ITPFEEK.M	0.75	112	Malate dehydrogenase, mitochondrial precursor
IPI00323592	K.ASIKK@GEDFVK.N	0.84	111	Malate dehydrogenase, mitochondrial precursor
Skeletal muscle				

liver				
Protein accession number	**Peptide sequence**	**log10(re-fed/fasted)**	**Index**	**Protein name**
Protein accession number	**Peptide sequence**	**log10(re-fed/fasted)**	**Index**	**Protein name**
IPI00127596	K.IEEIFK@K.A	−0.89	35	Creatine kinase M-type
IPI00221402	R.CVLK@IGEHTPSALAIMENANVLAR.Y	−0.83	79	Fructose-bisphosphate aldolase A
IPI00127596	R.FCVGLQK@IEEIFKK.A	−0.76	46	Creatine kinase M-type
IPI00125460	K.FDDPK@FEVIDK@PQS.-	0.85	25	ATP synthase coupling factor 6, mitochondrial precursor
Kidney				
Protein accession number	**Peptide sequence**	**log10(re-fed/fasted)**	**Index**	**Protein name**
IPI00118986	R.IGEK@YVDM#SAK.S	1.52	16	ATP synthase O subunit, mitochondrial precursor
IPI00154054	R.SK@EAWDAGKFASEITPITISVK.G	1.56	70	Acetyl-CoA acetyltransferase, mitochondrial precursor
IPI00230034	R.LCAATATILDK@PEDR.V	1.61	121	D-dopachrome decarboxylase
IPI00308885	K.EGFEK@ISK.G	1.76	95	60 kDa heat shock protein, mitochondrial precursor
IPI00134809	R.HKDAFLK@K.H	1.80	61	Dihydrolipoyllysine-residue succinyltransferase component of 2-oxoglutarate dehydrogenase complex, mitochondrial precursor
IPI00308885	R.SIAK@EGFEK.I	1.83	97	60 kDa heat shock protein, mitochondrial precursor
IPI00133903	R.HIVK@EFKR.E	1.87	85	Stress-70 protein, mitochondrial precursor
IPI00127625	R.DGLQNEK@SIVPTPVK.I	1.87	57	Hydroxymethylglutaryl-CoA lyase, mitochondrial precursor
Brain				
Protein accession number	**Peptide sequence**	**log10(re-fed/fasted)**	**Index**	**Protein name**
IPI00121440	R.VLAK@LAEK.E	0.96	11	Electron transfer flavoprotein subunit beta

Table 3

Enzymes, chaperones and carriers of bioenergetic metabolism showing differential acetylation between fasted and re-fed mice in different tissues. Proteins detected in more than one tissue are underlined.

Tissue	Mitochondrial					Cytosolic	
	FAO	TCA cycle	OxPh	Other	Transport	Glycolysis	Other
Kidney	ACAT1	α-KGDH	OSCP	HSP-60	-	-	DDT
		HMGCL		GRP-75			
Brown fat	TP-α	ACO2	-	GCSH	-	-	CYB5B
		HMGCL					
		PCCA-α					
Liver	ECH1	-	COX4	-	mVDAC1	ADH	CAT
			OSCP				
Muscle	-	-	F6	-	-	ALDOA	M-CK
Heart	-	MDH2	-	S-MtCK	mVDAC1	-	-
Brain	-	-	β-ETF	-	-	-	-

Abbreviations: Fatty acid oxidation (FAO), tricarboxylic acid cycle (TCA cycle), oxidative phosphorylation (OxPh), acetyl-CoA acetyltransferase (ACAT1), aconitase hydratase (ACO2), alcohol dehydrogenase (ADH), fructose-bisphosphate aldolase A (ALDOA), electron transfer flavoprotein subunit β (β-ETF), catalase (CAT), cytochrome c oxidase subunit 4 isoform 1 (COX4), cytochrome b5 type b (CYB5B), D-dopachrome decarboxylase (DDT), $\Delta^{3,5}$, $\Delta^{2,4}$-dienoyl-CoA isomerase (ECH1), ATP synthase coupling factor 6 (F6), glycine cleavage system H protein (GCSH), 75 kDa glucose-regulated protein/stress-70 protein (GRP-75), hydroxymethylglutaryl-CoA lyase (HMGCL), creatine kinase M type (M-CK), malate dehydrogenase (MDH2), α-ketoglutarate dehydrogenase complex (α-KGDH), oligomycin sensitivity conferral protein (OSCP), propionyl-CoA carboxylase α chain (PCCA-α), sarcomeric mitochondrial creatine kinase (S-MtCK), and trifunctional enzyme subunit α (TP-α).